Visualization of compensating currents in type-II/1 superconductor via high field cooling

Jacopo Valsecchi (iD), Jonathan S. White (iD), Marek Bartkowiak (iD), Wolfgang Treimer (iD), Youngju Kim, Seung Wook Lee (iD), Denis M. Gokhfeld (iD), Ralph P. Harti (iD), Manuel Morgano (iD), Markus Strobl (iD), and Christian Grünzweig

View Online   **Export Citation**   **CrossMark**

ARTICLES YOU MAY BE INTERESTED IN

Visualization of compensating currents in type-II/1 superconductor via high field cooling

Jacopo Valsecchi,[1,2,a] Jonathan S. White,[1] Marek Bartkowiak,[3] Wolfgang Treimer,[4] Youngju Kim,[5] Seung Wook Lee,[5] Denis M. Gokhfeld,[6] Ralph P. Harti,[1,2] Manuel Morgano,[1] Markus Strobl,[1] and Christian Grünzweig[1]

AFFILIATIONS

[1]Laboratory for Neutron Scattering and Imaging, Paul Scherrer Institut, 5232 Villigen, Switzerland
[2]University of Geneva, 1205 Geneva, Switzerland
[3]Laboratory for Neutron and Muon Instrumentation, Paul Scherrer Institut, 5232 Villigen, Switzerland
[4]University of Applied Sciences, Beuth Hochschule für Technik Berlin, 14109 Berlin, Germany
[5]School of Mechanical Engineering, Pusan National University, 46241 Busan, South Korea
[6]Kirensky Institute of Physics, Federal Research Center KSC SB RAS, 660036 Krasnoyarsk, Russia

[a]Author to whom correspondence should be addressed: jacopo.valsecchi@psi.ch

ABSTRACT

The morphology of vortex lattice domains in bulk type-II/1 superconductors is of central interest for many areas such as fundamental condensed matter physics, engineering science, and the optimization of materials for high transport current superconductivity applications. Here, we present a comprehensive experimental study of a single crystal niobium in the intermediate mixed state and Shubnikov phase with two complementary neutron techniques: high resolution polarized neutron imaging and small-angle neutron scattering. In this way, we were able to identify and visualize the occurrence of compensating currents, the flux line closure, and the freezing of the vortex spacing during the process of field cooling and high field cooling. With the combination of complementary neutron techniques, it was possible to add insights into the quest for the understanding of the flux pinning and nucleation of vortices in type-II/1 superconductors during the process of field cooling and high field cooling.

In the last decade, the spatial resolution capabilities of neutron imaging have brought additional insights into the investigation of magnetic phenomena in matter.[1–21] In particular, the thermodynamics of the phase transition between normal and superconducting states and also the flux pinning and trapping in superconductors due to the their peculiar nature of local magnetic interactions have spurred interest of neutron imaging researchers.[1,6,22–26]

Small-angle neutron scattering (SANS) is a well-known established method, which provides information about the size and shape of structures embedded in a homogeneous matrix. While SANS probes the Abrikosov vortex lattice (VL) and yields information, averaged over the illuminated region, about its morphology and spacing covering length scales from 10 to hundreds of nm, the polarized neutron imaging (PNI) technique allows us to assess complementary information about the magnetic field distributions.[27–29]

Superconductors are classified by the Ginzburg–Landau parameter κ into type-I ($\kappa < 1/\sqrt{2}$) and type-II ($\kappa > 1/\sqrt{2}$).[30,31] Here, the Ginzburg–Landau parameter is defined as $\kappa = \frac{\lambda_L}{\xi_{GL}}$, with λ_L being the London penetration depth and ξ_{GL} the superconducting coherence length. The phase diagram of type-II superconductors is characterized by the Meissner state (MS), which also occurs in type-I superconductors, and the Shubnikov phase (SH), aside from the normal conducting state (NS), as shown in Figs. 1(a) and 1(c). Furthermore, superconductors characterized by $\kappa \gtrsim 1/\sqrt{2}$, such as niobium, are subclassified as type-II/1, while $\kappa \gg 1/\sqrt{2}$ as type-II/2. The vortex lattice of type-II/1 superconductors shows both attractive and repulsive intervortex interaction components, as opposed to type-II/2, which is characterized by a purely repulsive behavior.[32] This peculiar behavior of the VL of type-II/1 superconductors can be observed in the intermediate mixed state (IMS), in which a domain structure develops in the form of a mixed
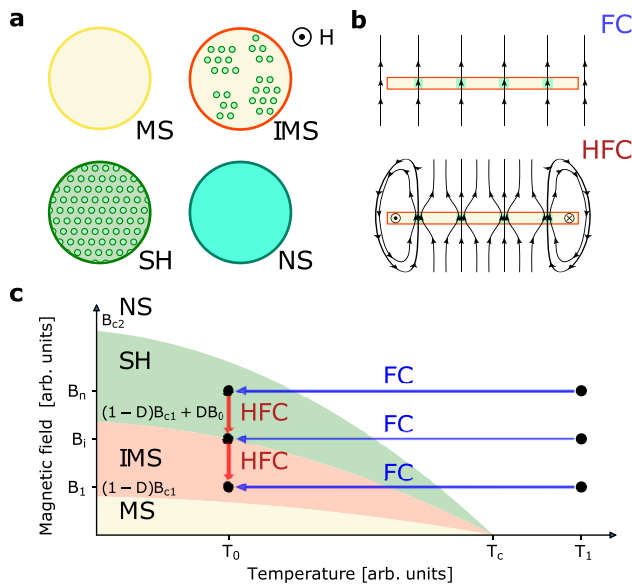
FIG. 1. (a) Illustration of the four different domain morphologies of a superconductor type-II/1 reached through the FC procedure: MS, IMS, SH, and NS, respectively. The external magnetic field H is applied perpendicular to the face of the disk. (b) Schematic illustration of the field distributions in the IMS in a superconductor type-II/1 disk for FC (top) and HFC (bottom). Particularly, the compensating currents, flux pinning, and line closure during the process of high field cooling HFC are depicted. The regions penetrated by magnetic fields are shown in green. The $\odot$ and $\otimes$ symbols show outgoing and incoming directions of the compensating currents. (c) Schematic phase diagram of a superconductor type-II/1 subdivided into MS, IMS, SH, and NS. The demagnetization factor (D) equals 0.88 for the probed specimen because the disk geometry is taken into account for the effective critical fields. The blue arrows depict different FC measurements at distinct magnetic fields B_1, B_i, and B_n, from $T_1 > T_c$ to $T_0 < T_c$, where T_c is the critical temperature. The red arrows depict the HFC measurements once the SH phase is accessed via the FC procedure at the specific external magnetic field B_n. The parameters B_0, B_{c1}, and B_{c2} are the constant magnetic induction, the lower critical field, and the upper critical field, respectively.

phase of the SH clusters and the MS regions, as depicted in Fig. 1(a). The origin and thermodynamics of the IMS have been the subject of numerous studies, and they are still a subject of investigations.[6,25–27]

A pivotal aspect of every investigation on the thermodynamics of type-II/1 superconductors is the cooling procedure adopted to access the superconductive phase, as depicted in Fig. 1(c). Recent investigations, based on a neutron multiscale approach, of the IMS state in niobium, focused on the process of field cooling (FC), have revealed an inhomogeneous domain structure of the VL and a universal temperature dependence of the vortex spacing, which is, however, independent of the external magnetic field.[25,26] A phenomenological explanation of the hysteretic behavior caused by pinning is provided by the Bean critical state model in type-II/1 superconductors assuming the existence of lossless critical currents, as depicted in Fig. 1(b).[33]

Here, we present an experimental study of the interplay of compensating currents, flux pinning, and line closure in a type-II/1 superconductor niobium during the process of FC and high field cooling (HFC). In order to extend the results of the previous investigations into the IMS, this study is based on the combination of magnetization,

SANS, and PNI measurements. The PNI technique is based on measuring variations of the neutron polarization, which undergoes a change in direction due to Larmor precession during the passage through a magnetic sample.[29,34] The polarization (P) can only be analyzed in relation to a specific direction (i.e., magnetic field orientation) and can be expressed as[29]

$$P = \frac{I_+ - I_-}{I_+ + I_-}, \tag{1}$$

where I_+ and I_- are the transmitted intensities measured behind a spin analyzer, with parallel $(+)$ and antiparallel $(-)$ alignment to the probed polarization direction. The precession angle ϕ is given by the path integral as follows:[28]

$$\phi = \omega_L t = \gamma_n Bt = \frac{\gamma_n}{v} \int B(s)ds = \frac{\gamma_n m_n \lambda}{h} \int B(s)ds, \tag{2}$$

where ω_L is the Larmor frequency, t is the time a neutron spends in the magnetic field B, γ_n is the gyromagnetic ratio of the neutron, v is the velocity, m_n is the neutron mass, λ is the wavelength, and h the is Planck constant. In order to detect a precession angle, the neutrons have to experience a non-adiabatic transition, which depends on the magnetic field gradient and neutron energy. The adiabatic regime is defined by the following condition:[18]

$$\frac{1}{B}\left(\frac{d\frac{B}{|B|}}{dt}\right) \ll \omega_L. \tag{3}$$

The FC and HFC cooling procedures applied for both the SANS and PNI measurements are depicted in Fig. 1(c). The FC procedure consists of ramping up the external magnetic field at a temperature of 12 K (T_1), above the critical temperature ($T_c = 9.25$ K for Nb), and cooling the sample down to 4 K (T_0), below the critical temperature, for each measured field. Scanning through the HFC procedure starts with the access to the SH phase from T = 12 K to T = 4 K at B = 80 mT, in a similar manner like FC at the same field, and subsequently, the external magnetic field is ramped down step by step for consecutive measurements, while the temperature is kept constant.

The sample is a low purity single crystal disk of niobium with 12 mm diameter, 2 mm thickness, and a residual resistivity ratio (RRR) of $\approx$10, which has been characterized by a quantum design physical property measurement system (PPMS). The $\langle 111 \rangle$ crystallographic axis is perpendicular to the face of the Nb disk. This kind of low purity specimen can be considered a realistic model material for practical applications of superconductors.

The magnetization curves of the Nb sample are shown in Fig. 2 as a function of the applied magnetic field, perpendicular to the face of the disk, for various temperatures between 4 and 9 K. Such magnetization curves are typical for type-II/1 superconductors: the behavior of the magnetization hysteresis loop is determined by an entrance of the VL into the sample and by trapping the magnetic field. The broad hysteresis loop is characteristic of a strong pinning behavior, a hallmark of superconductors with a low RRR. The demagnetization factor (D) for a disk with the magnetic field applied along the cylindrical axis has been estimated to be $\approx$0.88, calculated according to[28]
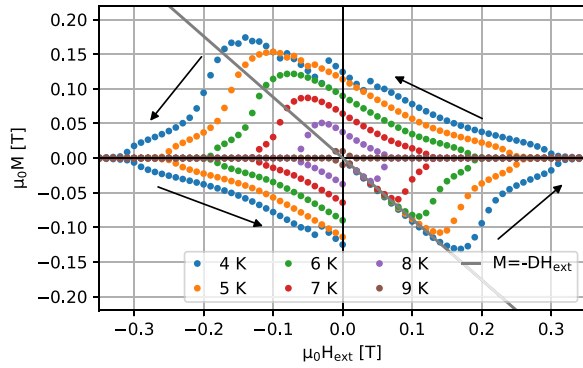
FIG. 2. PPMS data of the Nb disk. Magnetization as a function of the applied external magnetic field perpendicular to the face of the disk, measured for different temperatures between 4 K and 9 K in the range between ± 350 mT. Here, the initial magnetization curves after zero field cooling (ZFC) and three quarter of a hysteresis loop are shown. The demagnetization factor D is shown in gray as $M = -DH_{ext} = -0.88H_{ext}$.

$$D = 1 - \frac{1}{1 + \left(\frac{r}{h}\right)q},$$

$$q = \frac{4}{3\pi} + \frac{2}{3\pi}\tan\left(\frac{h}{r}\ln\left(1 + \frac{r}{h}\right)^{1.27}\right),$$

(4)

where r and h are the radius and the thickness of the cylinder. The SANS measurements have been carried out at SANS-I, at PSI, via rocking scans over $\pm 2°$. The data have been corrected for a high temperature background using a background measurement in the normal state. The external magnetic field is applied along the neutron beam direction and perpendicular to the face of the Nb disk. A sixfold pattern is observed for the illuminated area of the sample, corresponding to the central inner part of the Nb disk ≈ 8 mm in diameter, as expected from the literature.[6,27] The properties of the VL extracted from the SANS during the FC measurements, depicted in Fig. 3(a), show a plateau in the IMS state and the characteristic $g_{VL} \propto \sqrt{B}$ behavior in the SH phase for magnetic field $B \gtrsim H_c \approx 45$ mT, in agreement with the literature.[6,25–27] Here, g_{VL} is the reciprocal lattice vector, i.e., the inverse of the vortex lattice parameter a_{VL}, and can be expressed as[25]

$$g_{VL} = \frac{4\pi}{\sqrt{3}a_{VL}} = \sqrt{\frac{8\pi^2 B_{int}}{\sqrt{3}\Phi_0}},$$

(5)

where Φ_0 is the magnetic flux quantum and B_{int} depends on the demagnetization D of the sample. However, in the probed magnetic field range, the sample does not show the characteristic drop at a very low field due to the flux expulsion in the MS, mainly due to pinning and impurities, yellow region in Fig. 3(a). This does not allow us to estimate the value of the field for the IMS-MS phase transition. The field dependence of the integrated scattering intensity in the FC measurements, as illustrated in Fig. 3(b), shows the characteristic peak at the IMS-SH phase transition, in good agreement with the literature.[6,25–27,35] The HFC measurements, on the other hand, show a freezing of g_{VL} at the initial value, i.e., when the superconducting phase
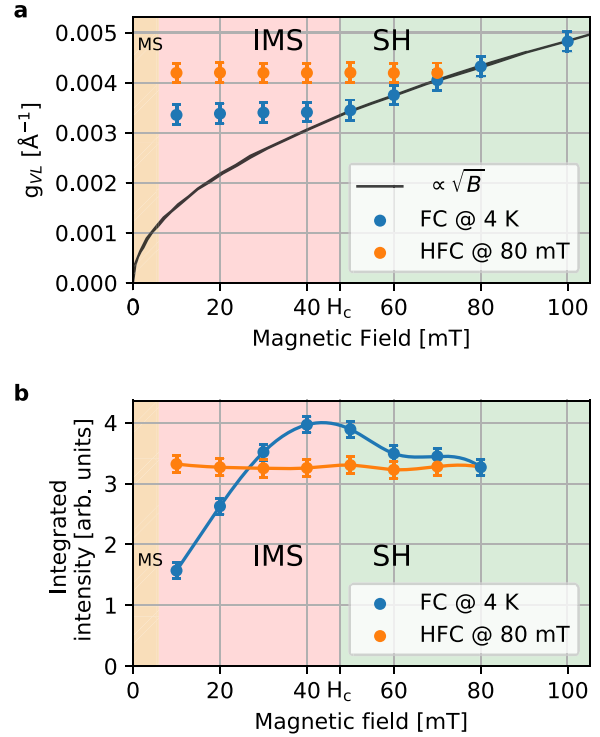

FIG. 3. SANS results. (a) Reciprocal lattice vector g_{VL} measured by SANS as a function of increasing and decreasing applied magnetic fields through FC (blue) and HFC (orange). For a high field, the FC data points are proportional to $\sqrt{B}$, characteristic of the SH phase. (b) Integrated scattering intensity curves. The blue data points have been acquired via independent FC procedures. The orange data points have been measured via the HFC procedure. $H_c \approx 45$ mT defines the boundary between IMS (red) and SH (green). The MS (yellow) has not been probed during the SANS measurements.

is accessed at 80 mT, without exhibiting any discontinuities throughout the SH-IMS phase transition. In a similar manner, the integrated intensity distribution, which is proportional to the magnetic flux structures in the sample, is constant for HFC, as shown in Fig. 3(b), and indicates no nucleation process of vortex domains, in agreement with the results reported by Bykov *et al.*[35]

The PNI measurements have been carried out at the polarized cold neutron beamline BOA, at PSI.[36] The monochromatic neutron beam is polarized along the vertical axis with an overall polarization of $\approx 90\%$ at $\lambda = 3.5$ Å. A spatial resolution of 130 μm has been measured with a Siemens star test object.[37] The cryomagnet used for the measurements generates a magnetic field that is aligned along the propagation direction of the neutrons, and it is adiabatically coupled with the incoming neutron spin polarization and the spin analyzer. A complete sequence covering the magnetic field ranging from 20 mT to 80 mT has been acquired for both FC and HFC. In Figs. 4(a)–4(d), a selection of images is shown. Throughout the whole FC procedure, only a weak signal has been detected, visible only at the edge of the disk, as shown in Figs. 4(a) and 4(e). This indicates that during the SH-IMS phase transition in the FC procedure, the neutron polarization is adiabatically coupled, as defined in Eq. (3), with the external magnetic field applied to the sample, which, thus, has no
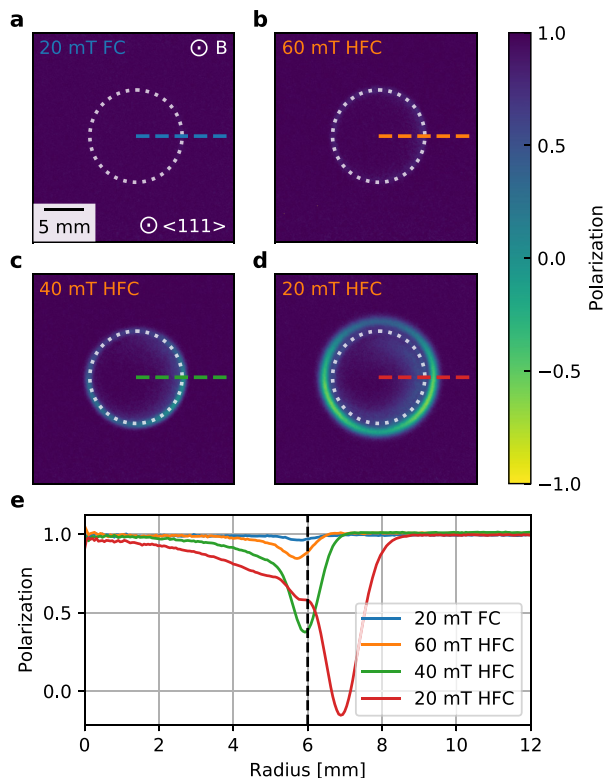
FIG. 4. (a) PNI for FC at 20 mT and 4 K in the IMS phase. (b)–(d) PNI for HFC at 60 mT, 40 mT, and 20 mT, respectively. The color-coded dashed lines show the extension of the integrated radial profiles for each of the FC and HFC measurements shown in (e). The dashed circle indicates the Nb disk. The external magnetic field is applied along the beam direction, parallel to the ⟨111⟩ axis and perpendicular to the disk face. (e) Neutron polarization profiles of the FC and HFC radial profiles, color-coded according to (a)–(d). The vertical dashed line depicts the edge of the sample.

perpendicular component to the polarization vector; hence, no spin flipping precession occurs and the polarization is equal to $+1$, as shown in Fig. 4(a).[29] Hence, it serves as the reference point for the comparison of the images acquired during the HFC hysteresis loop. The PNI images of the HFC, on the other hand, show a field dependent behavior emerging at the periphery of the disk, as illustrated in Figs. 4(b)–4(d). This local decrease in polarization during the HFC becomes more pronounced for weaker fields, and it shifts toward larger radii, extending beyond the edge of the Nb disk, as shown in Figs. 4(d) and 4(e). The fact that a polarization of $P \approx 0\%$ is reached, as illustrated in Fig. 4(e) for the case of HFC at 20 mT, indicates a non-adiabatic transition, according to Eq. (3), due to the strong gradient generated by the swirling of the magnetic field, as depicted in Fig. 1(b).

While the VL cannot be directly resolved in real space by PNI, a comprehensive interpretation of the VL structure can be inferred via the SANS results, which show the characteristic SH-IMS phase transition in FC followed by the subsequent nucleation of an irregular domain structure. In contrast, for HFC, no signs of the SH-IMS phase transition have been observed experimentally, and g_{VL} and the

integrated scattering intensity indicate a freezing of the VL at the initial value of the thermodynamic path, which does not lead to a vortex domain formation, mainly due to pinning. The PNI results do not show a stationary system during the freezing of the VL for HFC, and a clear field dependent ring appears, which protrudes beyond the edge of the disk. Since circulating currents appear only during ZFC, the signal induced by the HFC procedure leads to the compensating currents and the flux line closure as depicted in Fig. 1(b). A similar situation has been observed using the Faraday effect in high T_c superconductors.[38]

In conclusion, we have shown how the combination of the results obtained with two complementary neutron techniques, SANS and PNI, provides additional insights into the thermodynamics of low purity type-II/1 superconductors by characterizing the VL throughout the thermodynamic path and visualizing the occurrence of compensating currents and flux line closure.

See the supplementary material for the SANS diffraction patterns and for the complete dataset of the PNI images.

DATA AVAILABILITY

The data that support the findings of this study are available from the corresponding author upon reasonable request.

REFERENCES

[1] N. Kardjilov, I. Manke, M. Strobl, A. A. Hilger, W. Treimer, M. Meissner, T. Krist, and J. Banhart, "Three-dimensional imaging of magnetic fields with polarized neutrons," Nat. Phys. **4**, 399–403 (2008).

[2] C. Grünzweig, C. David, O. Bunk, M. Dierolf, G. Frei, G. Kühne, R. Schäfer, S. Pofahl, H. M. Rønnow, and F. Pfeiffer, "Bulk magnetic domain structures visualized by neutron dark-field imaging," Appl. Phys. Lett. **93**, 112504 (2008).

[3] F. M. Piegsa, B. van den Brandt, P. Hautle, J. Kohlbrecher, and J. A. Konter, "Quantitative radiography of magnetic fields using neutron spin phase imaging," Phys. Rev. Lett. **102**, 145501 (2009).

[4] I. Manke, N. Kardjilov, R. Schäfer, A. Hilger, M. Strobl, M. Dawson, C. Grünzweig, G. Behr, M. Hentschel, C. David, A. Kupsch, A. Lange, and J. Banhart, "Three-dimensional imaging of magnetic domains," Nat. Commun. **1**, 125 (2010).

[5] S. W. Lee, K. Y. Kim, O. Y. Kwon, N. Kardjilov, M. Dawson, A. Hilger, and I. Manke, "Observation of magnetic domains in insulation-coated electrical steels by neutron dark-field imaging," Appl. Phys. Express **3**, 106602 (2010).

[6] T. Reimann, S. Mühlbauer, M. Schulz, B. Betz, A. Kaestner, V. Pipich, P. Böni, and C. Grünzweig, "Visualizing the morphology of vortex lattice domains in a bulk type-II superconductor," Nat. Commun. **6**, 8813 (2015).

[7] A. S. Tremsin, N. Kardjilov, M. Strobl, I. Manke, M. Dawson, J. B. McPhate, J. V. Vallerga, O. H. W. Siegmund, and W. B. Feller, "Imaging of dynamic magnetic fields with spin-polarized neutron beams," New J. Phys. **17**, 043047 (2015).

[8] M. Schulz, A. Neubauer, P. Böni, and C. Pfleiderer, "Neutron depolarization imaging of the hydrostatic pressure dependence of inhomogeneous ferromagnets," Appl. Phys. Lett. **108**, 202402 (2016).

[9]B. Betz, P. Rauscher, R. P. Harti, R. Schäfer, H. Van Swygenhoven, A. Kaestner, J. Hovind, E. Lehmann, and C. Grünzweig, "In-situ visualization of stress-dependent bulk magnetic domain formation by neutron grating interferometry," Appl. Phys. Lett. **108**, 012405 (2016).

[10]B. Betz, P. Rauscher, R. P. Harti, R. Schäfer, A. Irastorza-Landa, H. Van Swygenhoven, A. Kaestner, J. Hovind, E. Pomjakushina, E. Lehmann, and C. Grünzweig, "Magnetization response of the bulk and supplementary magnetic domain structure in high-permeability steel laminations visualized in situ by neutron dark-field imaging," Phys. Rev. Appl. **6**, 024023 (2016).

[11]B. Betz, P. Rauscher, R. P. Harti, R. Schäfer, H. Van Swygenhoven, A. Kaestner, J. Hovind, E. Lehmann, and C. Grünzweig, "Frequency-induced bulk magnetic domain-wall freezing visualized by neutron dark-field imaging," Phys. Rev. Appl. **6**, 024024 (2016).

[12]P. Rauscher, B. Betz, J. Hauptmann, A. Wetzig, E. Beyer, and C. Grünzweig, "The influence of laser scribing on magnetic domain formation in grain oriented electrical steel visualized by directional neutron dark-field imaging," Sci. Rep. **6**, 38307 (2016).

[13]R. P. Harti, M. Strobl, R. Schäfer, N. Kardjilov, A. S. Tremsin, and C. Grünzweig, "Dynamic volume magnetic domain wall imaging in grain oriented electrical steel at power frequencies with accumulative high-frame rate neutron dark-field imaging," Sci. Rep. **8**, 15754 (2018).

[14]M. Sales, M. Strobl, T. Shinohara, A. Tremsin, L. T. Kuhn, W. R. B. Lionheart, N. M. Desai, A. B. Dahl, and S. Schmidt, "Three dimensional polarimetric neutron tomography of magnetic fields," Sci. Rep. **8**, 2214 (2018).

[15]A. Hilger, I. Manke, N. Kardjilov, M. Osenberg, H. Markötter, and J. Banhart, "Tensorial neutron tomography of three-dimensional magnetic vector fields in bulk materials," Nat. Commun. **9**, 4023 (2018).

[16]M. Sales, T. Shinohara, M. K. Sorensen, E. B. Knudsen, A. Tremsin, M. Strobl, and S. Schmidt, "Three dimensional polarimetric neutron tomography— Beyond the phase-wrapping limit," J. Phys. D: Appl. Phys. **52**, 205001 (2019).

[17]P. Jorba, M. Schulz, D. S. Hussey, M. Abir, M. Seifert, V. Tsurkan, A. Loidl, C. Pfleiderer, and B. Khaykovich, "High-resolution neutron depolarization microscopy of the ferromagnetic transitions in Ni3Al and HgCr$_2$Se$_4$ under pressure," J. Magn. Magn. Mater. **475**, 176–183 (2019).

[18]J. Valsecchi, R. P. Harti, M. Raventós, M. D. Siegwart, M. Morgano, P. Boillat, M. Strobl, P. Hautle, L. Holitzner, U. Filges, W. Treimer, F. M. Piegsa, and C. Grünzweig, "Visualization and quantification of inhomogeneous and anisotropic magnetic fields by polarized neutron grating interferometry," Nat. Commun. **10**, 3788 (2019).

[19]Y. Kim, J. Kim, D. S. Hussey, O. Y. Kwon, and S. W. Lee, "Visualization of magnetic domains in electrical steel using high-resolution dark-field imaging," Korean J. Met. Mater. **57**, 352–359 (2019).

[20]I. Dhiman, R. Ziesche, L. Riik, I. Manke, A. Hilger, B. Radhakrishnan, T. Burress, W. Treimer, and N. Kardjilov, "Visualization of magnetic domain structure in FeSi based high permeability steel plates by neutron imaging," Mater. Lett. **259**, 126816 (2020).

[21]T. Neuwirth, A. Backs, A. Gustschin, S. Vogt, F. Pfeiffer, P. Böni, and M. Schulz, "A high visibility Talbot-Lau neutron grating interferometer to investigate stress-induced magnetic degradation in electrical steel," Sci. Rep. **10**, 1764 (2020).

[22]W. Treimer, O. Ebrahimi, and N. Karakas, "Observation of partial Meissner effect and flux pinning in superconducting lead containing non-superconducting parts," Appl. Phys. Lett. **101**, 162603 (2012).

[23]W. Treimer, O. Ebrahimi, N. Karakas, and R. Prozorov, "Polarized neutron imaging and three-dimensional calculation of magnetic flux trapping in bulk of superconductors," Phys. Rev. B **85**, 184522 (2012).

[24]I. Dhiman, R. Ziesche, V. K. Anand, L. Riik, G. Song, A. T. M. N. Islam, I. Tanaka, and W. Treimer, "Thermodynamics of Meissner effect and flux pinning behavior in the bulk of single-crystal LaSrCuO," Phys. Rev. B **96**, 104517 (2017).

[25]T. Reimann, M. Schulz, D. F. Mildner, M. Bleuel, A. Brûlet, R. P. Harti, G. Benka, A. Bauer, P. Böni, and S. Mühlbauer, "Domain formation in the type-II/1 superconductor niobium: Interplay of pinning, geometry, and attractive vortex-vortex interaction," Phys. Rev. B **96**, 144506 (2017).

[26]A. Backs, M. Schulz, V. Pipich, M. Kleinhans, P. Böni, and S. Mühlbauer, "Universal behavior of the IMS domain formation in superconducting niobium," Phys. Rev. B **100**, 064503 (2019).

[27]S. Mühlbauer, C. Pfleiderer, P. Böni, M. Laver, E. M. Forgan, D. Fort, U. Keiderling, and G. Behr, "Morphology of the superconducting vortex lattice in ultrapure niobium," Phys. Rev. Lett. **102**, 136408 (2009).

[28]W. Treimer, "Radiography and tomography with polarized neutrons," J. Magn. Magn. Mater. **350**, 188–198 (2014).

[29]M. Strobl, H. Heimonen, S. Schmidt, M. Sales, N. Kardjilov, A. Hilger, I. Manke, T. Shinohara, and J. Valsecchi, "Polarization measurements in neutron imaging," J. Phys. D: Appl. Phys. **52**, 123001 (2019).

[30]V. L. Ginzburg and L. D. Landau, "On the theory of superconductivity," Zh. Eksp. Teor. Fiz. **20**, 1064–1082 (1950).

[31]A. A. Abrikosov, "On the magnetic properties of superconductors of the second group," Zh. Eksp. Teor. Fiz. **32**, 1174–1182 (1957).

[32]A. Vagov, A. A. Shanenko, M. V. Milošević, V. M. Axt, V. M. Vinokur, J. A. Aguiar, and F. M. Peeters, "Superconductivity between standard types: Multiband versus single-band materials," Phys. Rev. B **93**, 174503 (2016).

[33]C. P. Bean, "Magnetization of hard superconductors," Phys. Rev. Lett. **8**, 250–253 (1962).

[34]N. M. Desai, W. R. B. Lionheart, M. Sales, M. Strobl, and S. S. Schmidt, "Polarimetric neutron tomography of magnetic fields: Uniqueness of solution and reconstruction," Inverse Probl. **36**, 045001 (2020).

[35]A. A. Bykov, D. M. Gokhfeld, E. V. Altynbaev, K. Y. Terent'ev, N. Martin, S. V. Semenov, and S. V. Grigoriev, "Effect of trapped magnetic flux on neutron scattering in La$_{1.85}$Sr$_{0.15}$CuO$_4$ superconductor," J. Supercond. Novel Magn. **32**, 3797–3802 (2019).

[36]M. Morgano, S. Peetermans, E. Lehmann, T. Panzner, and U. Filges, "Neutron imaging options at the BOA beamline at Paul Scherrer Institut," Nucl. Instrum. Methods Phys. Res., Sect. A **754**, 46–56 (2014).

[37]C. Grünzweig, G. Frei, E. Lehmann, G. Kühne, and C. David, "Highly absorbing gadolinium test device to characterize the performance of neutron imaging detector systems," Rev. Sci. Instrum. **78**, 053708 (2007).

[38]T. Schuster, M. R. Koblischka, B. Ludescher, and H. Kronmüller, "Observation of inverse domains in high TC superconductors," J. Appl. Phys. **72**, 1478–1485 (1992).